Design and Development of a Temperature Control System for Blood Optical

Characterization

Dawson Garner

A senior thesis submitted to the faculty of
Brigham Young University
in partial fulfillment of the requirements for the degree of

Bachelor of Science

Robert Davis and Richard Vanfleet, Advisors

Department of Physics and Astronomy

Brigham Young University

ABSTRACT

Design and Development of a Temperature Control System for Blood Optical Characterization

Dawson Garner
Department of Physics and Astronomy, BYU
Bachelor of Science

This thesis presents the design and validation of a temperature control system for bioptics experiments involving whole blood. The system was developed to simulate physiologically relevant thermal conditions and maintain stable temperatures between 36°C and 40°C over extended durations. A six-thermistor monitoring array was constructed to track spatial temperature distribution within the experimental enclosure, and custom Python software was implemented to log real-time data and visualize thermal behavior. To eliminate signal interference between thermistor channels, the data acquisition code was redesigned to sample sequentially, resolving crosstalk issues and restoring sensor independence. A custom foamcore heat box was constructed to surround the optical setup, with cotton insulation added to reduce thermal leakage through the base and cable ingress points. Iterative tuning of the Arduino-based PID controller enabled reliable heating input, with optimal performance achieved when set to 50°C. Results showed that the insulated system maintained thermal consistency across the experimental plane within a narrow two-degree range, compared to over ten degrees in the uninsulated case. These outcomes demonstrate the system's suitability for long-duration, temperature-sensitive optical measurements and provide a low-cost, modular framework for thermal regulation in bioptic research environments.

ACKNOWLEDGMENTS

I would like to express my sincere gratitude to my advisors, Dr. Robert Davis and Dr. Richard Vanfleet, for their exceptional guidance, support, and mentorship throughout the course of this project. I am also grateful to Professor Chanel Earl for her valuable assistance in the organization and editing of this thesis. I extend my appreciation to the members of my research group—Rees Stenson, Jared Roth, and Jared Logan—for their collaboration and insight, and to my family and friends for their constant encouragement and support during this endeavor.

Contents

Chapter 1

Introduction

Understanding how light interacts with biological tissue is essential for advancing non-invasive medical diagnostics. One particularly important area of study involves analyzing how whole blood absorbs and scatters light in the near-infrared (NIR) spectrum. This project focuses on the development of a temperature control system capable of maintaining physiologically relevant conditions for optical experiments involving whole blood. The central goal is to enable future studies on how temperature influences the optical absorption properties of blood, with the broader aim of supporting advancements in medical diagnostics.

The optical behavior of blood is governed by its physiological composition, which includes red blood cells (RBCs), plasma, and water. Scattering of light arises from differences in refractive indices between these components, while absorption is primarily driven by chromophores like hemoglobin and water. These properties vary with several physiological factors—including wavelength [1], oxygenation [5,6], hematocrit [2,3], and temperature [3,6]—making blood a complex but highly valuable model for optical study.

Light interaction with tissue can be described by the Beer-Lambert law:

$$I_t = I_0 e^{-x(\mu_s + \mu_a)}$$

where I_0 is the incident light intensity, I_t is the transmitted intensity, x is the path length, and μ_s and μ_a are the scattering and absorption coefficients, respectively. These coefficients quantify how much light is lost due to scattering and absorption as it passes through a medium. The reduced scattering coefficient, $\mu'_s = (1-g)\mu_s$, accounts for the angular distribution of scattering, where g is the anisotropy factor.

Several foundational studies have shaped current understanding of blood's optical properties and inform the design of this project. Early work by Yaroslavsky et al. [1] used double-integrating sphere measurements and inverse Monte Carlo simulations to characterize the scattering and absorption coeffecients of blood in the near-infrared (NIR) range. Their findings highlighted the distinct optical behavior of blood compared to other tissues, as well as the sensitivity of derived properties to the scattering phase function model—emphasizing the need for precision in experimental design.

Building on this foundation, Amerov et al. [2] extended the analysis across a wider spectral range (up to 2500 nm), identifying hemoglobin and water as the primary absorbers and confirming that blood's scattering follows a wavelength-dependent trend approximately proportional to $\lambda^{-1.7}$. They also demonstrated that physiological parameters like hematocrit and oxygen saturation substantially impact absorption, making clear the importance of environmental and biological conditions in optical measurements.

This emphasis on physiological factors was furthered by Bosschaart et al. [3], who specifically investigated the temperature dependence of blood's optical behavior from 500 to 1100 nm. They found that the most significant temperature-induced changes arose from water absorption, particularly near 960 nm. Their results motivated the need to extend thermal studies to longer wavelengths and highlighted the practical challenges of measuring temperature effects in whole blood—rather than in simplified or isolated blood components.

Complementary to these studies, Friebel and Meinke [5] examined how the absorption behavior of hemoglobin changes with concentration and oxygenation state. They validated the use of Beer-

Lambert law at high hemoglobin concentrations and identified a stable isosbestic point at 805 nm, reinforcing the role of hemoglobin as a consistent diagnostic marker. Their work supports the assumption that absorption behavior in whole blood remains linear and interpretable even under varying physiological conditions.

Finally, Sfareni and Quaresima [6] provided direct insight into the temperature sensitivity of hemoglobin spectra across its oxygenation states. They observed that while oxy- and methemoglobin absorption changed minimally with temperature, deoxyhemoglobin exhibited a measurable reduction in absorption intensity—underscoring the need to control and monitor thermal conditions during spectroscopic measurements.

Together, these studies establish a clear trajectory: from foundational spectral characterization, through recognition of key physiological dependencies, to the realization that temperature must be carefully regulated in blood optics research. This thesis builds on that trajectory by developing a system designed to meet the experimental demands of future temperature-sensitive optical measurements in whole blood.

While previous studies have highlighted the importance of controlling physiological variables like temperature during optical measurements of blood, less attention has been given to the practical development of systems capable of maintaining such control in a laboratory setting. In particular, achieving stable, physiologically relevant temperatures across a complex optical setup—such as the one used at BYU for tissue optics measurements involving integrating spheres and dynamic flow systems—remains a technical challenge. To support future investigations into temperature-dependent optical behavior, a robust and consistent temperature control system is essential.

The purpose of this project is to design, refine, and implement such a system. This includes enhancing the pre-existing thermistor monitoring network by expanding from four to six sensors, resolving data interference across channels in the DAQ system, constructing and insulating a custom heat box to enclose the optical experiment, and calibrating the heating input to achieve and maintain

biologically relevant temperatures. Each of these improvements was iteratively tested and optimized to ensure system stability, accuracy, and reproducibility. Ultimately, this work lays the groundwork for future studies on the temperature dependence of blood's optical properties by providing a system capable of maintaining constant physiological temperatures, thereby contributing to the broader goal of enabling more reliable experimentation within bioptics.

This project builds on foundational work completed by Jared Roth, who originally constructed the foamcore enclosure and installed the perforated ceiling for airflow distribution. The Arduino-based PID controller and the dehydrator-fan heating system were conceived and implemented by Dr. Richard Vanfleet. The issue of thermistor signal interference was identified with the assistance of Jared Logan, whose insight helped resolve critical data acquisition problems. Additional improvements to the thermal insulation of the enclosure were made with the help of Rees Stenson and Jared Roth.

Chapter 2

Methods

2.1   System Objectives and Design Constraints

The objective of this project was to develop a temperature control system capable of maintaining physiologically relevant conditions for a bioptic experiment simulating human body temperature. The system is intended to support experiments involving the optical characterization of whole blood, where temperature stability is essential to reducing thermal noise. The design—mimicking in vivo conditions—aimed to maintain blood temperature within approximately ± 1°C of a target value—ideally within 1°C, but with up to 2°C variation still considered acceptable—over extended periods, potentially lasting as long as eight hours.

Several practical constraints guided the system's construction. These included the physical overhang of the optical table, which limited the allowable height of the enclosure; the spatial footprint of the experiment itself, which required the thermal box to fit as tightly as possible around the experimental region; the need for the enclosure to be lightweight and easily removable for access and adjustments; and the requirement for a material that would provide strong thermal insulation while remaining simple to build with. These factors led to the selection of foamcore, which was

reinforced with painter's tape for structure and sealed edges. The final enclosure also interfaced with an Arduino-based PID controller and LCD screen to allow manual temperature regulation. Success for the system was defined by its ability to maintain thermal consistency within the target range under realistic experimental conditions involving flow, heat loss, and environmental exposure.

2.2 Thermistor Network Expansion and DAQ Integration

To monitor the temperature at various locations within the enclosure, a network of six thermistors was implemented. These thermistors—marketed as 100K 3950 NTC sensors—were selected for their sensitivity and ease of integration. Although the system initially employed four sensors, they were all replaced to ensure that identical hardware and calibration profiles were used across the expanded six-point configuration. Each thermistor was calibrated individually by determining its Steinhart-Hart coefficients, a process that enabled consistent and accurate temperature readings across the setup.

Calibration was performed using an ANOVA Precision Cooker Nano 3.0 to precisely control the temperature of a water bath. Each thermistor (sealed in plastic bags) was submerged in the bath alongside a reference thermometer, and resistance readings were recorded at specific temperature intervals. From 20°C to 36°C, resistance values were measured at 4°C increments. From 36°C to 40°C—a physiologically critical range for blood experiments—measurements were taken at 1°C intervals to maximize resolution. Additional calibration points were collected at 44°C and 48°C to expand the usable temperature range of the system.

These temperature-resistance pairs were then used to compute the three Steinhart-Hart coefficients (A, B, and C) for each thermistor. The standard Steinhart-Hart equation was employed:

$$\frac{1}{T} = A + B\ln(R) + C\left(\ln(R)\right)^3$$

where T is the temperature in Kelvin and R is the measured resistance in ohms. By performing a nonlinear regression on the calibration data, the optimal coefficients were derived to fit the equation for each sensor. These coefficients were then hard-coded into the software, enabling real-time conversion from measured voltage to accurate temperature for each thermistor during experimental runs.

These sensors were integrated into a National Instruments DAQ system (model USB-6211), but the increased number of channels and the frequency of data acquisition quickly revealed a technical limitation. When the DAQ attempted to collect simultaneous temperature data from all six thermistors every half second, the resulting values showed irregular interference. Specifically, when a single thermistor registered a sharp increase—such as from being touched by a human hand—corresponding tugs appeared in the data of the other channels, even though no actual thermal change had occurred in those regions. This phenomenon indicated that data from one channel was bleeding into others, compromising the accuracy of the system.

To resolve this issue, the Python code used to collect and log thermistor data was rewritten to adopt a sequential sampling approach. Instead of reading all six channels at once, the code now cycles through each thermistor one at a time, recording a value for each every second. Since real-time synchronization of all sensors was not essential for the application—only a general spatial profile of the temperature distribution was needed—this adjustment eliminated interference and restored reliable temperature readings across the system. This approach ensured that each thermistor independently reported localized temperatures in the plane of the blood flow path, which includes tubing, flow chambers, and reservoirs situated between pairs of integrating spheres in both experimental branches.

2.3   Heat Box Construction and Circulation Design

To create a thermally stable environment around the optical setup, a heat box was constructed using foamcore. The structure was open at the bottom and was designed to enclose the entire region of interest, including the blood reservoirs housed in a water bath, the syringe pump driving flow, and the tubing and flow chambers connecting each component. The box fully covered both the experimental and control branches, each of which contains two integrating spheres with flow chambers positioned in between.

The enclosure stood just under two feet tall and slightly more than two feet wide, carefully measured to accommodate the optical system while fitting beneath the overhanging support structure on the lab bench (see Figure 2.1). At the top of the box, a fan was installed in a cutout, forming the centerpiece of the thermal distribution system. This fan—pumped with heat from components of a repurposed dehydrator—blew downward into the interior of the box, pushing warm air throughout the volume and forcing it down to the experimental plane. A second internal layer, positioned just beneath the fan, served as a perforated ceiling. Holes were manually cut into this surface to allow airflow and improve thermal mixing (see Figure 2.3). This two-tier design leveraged basic principles of pressure and fluid dynamics to create a more uniform distribution of heat, preventing hotspots and stagnation.
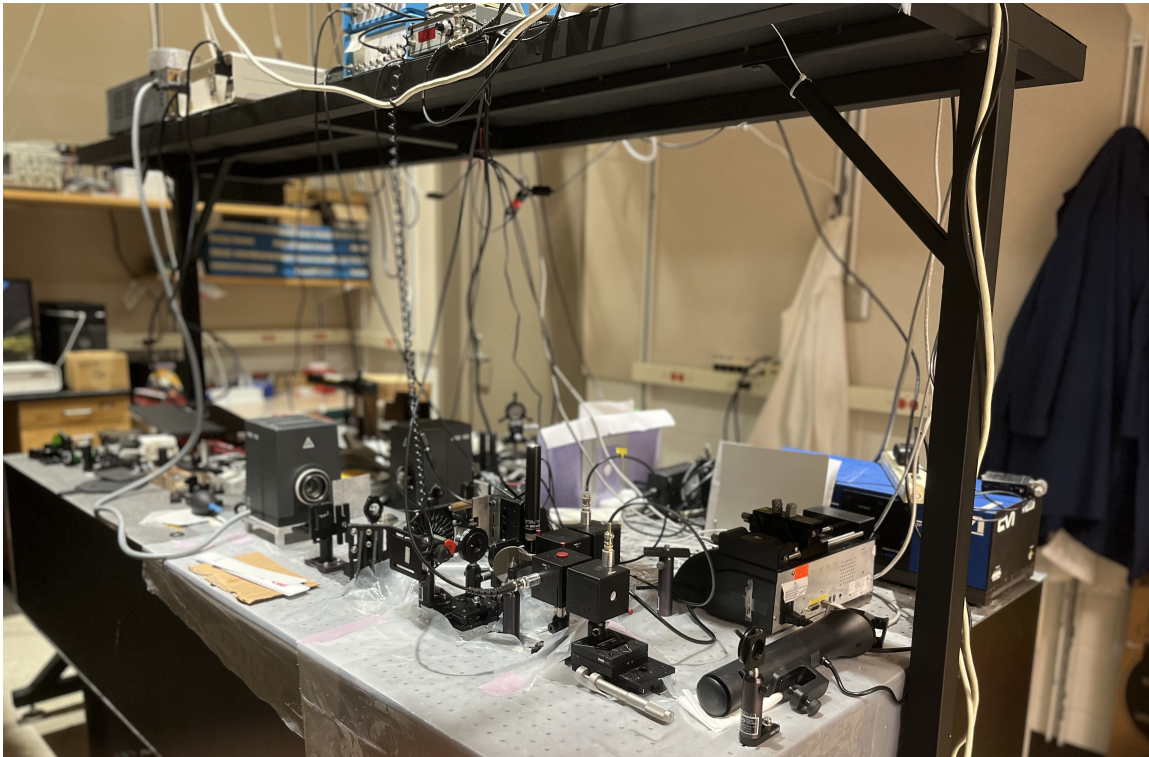
Figure 2.1 Photograph of the optical table and support overhang used for the blood optics experiment. The enclosure was designed to fit precisely within this constrained space (the closest quarter of the table to the image), surrounding the experimental region while allowing access to cabling and flow components.

Figure 2.2 Photograph of the front-facing side of the insulated heat box. The cut-out labeled "Door" provides an access point for observing or adjusting the optical experiment inside without removing the entire enclosure. Cotton insulation is visible at the some of the openings, helping seal gaps and improve thermal retention. Wiring from the fan and thermistor array exits through the top of the box.
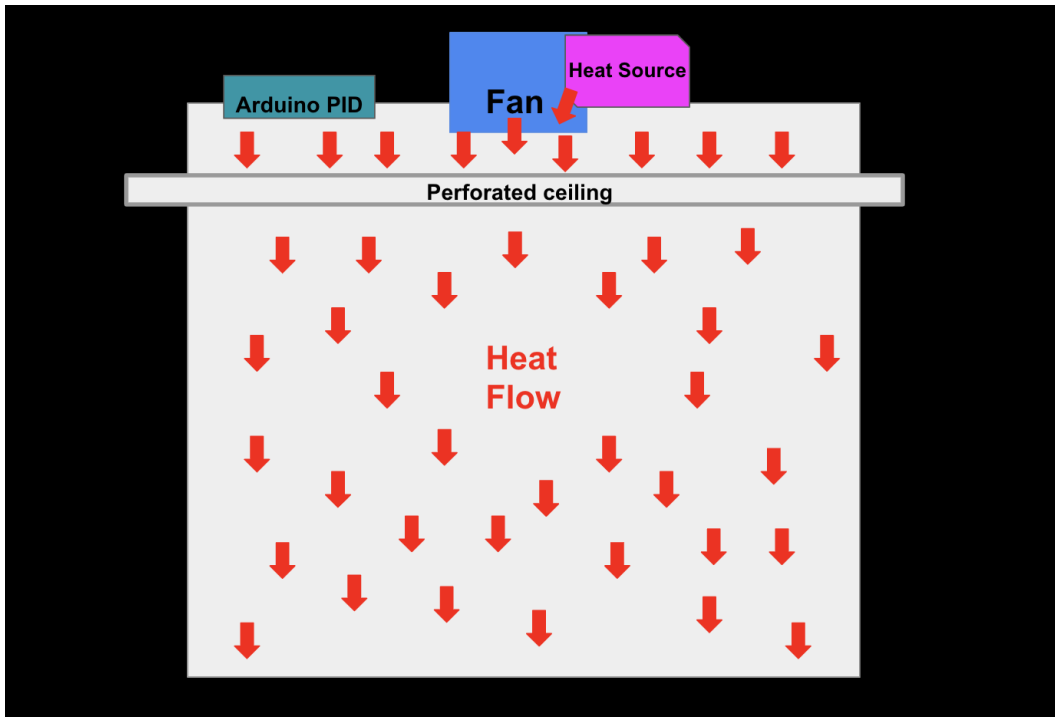
Figure 2.3 Cross-sectional sketch of the insulated enclosure showing the downward-blowing fan, perforated internal ceiling, and overall airflow distribution. Warm air enters from the top and circulates downward through manually cut holes to achieve uniform heat distribution across the experimental plane.

The entire box was hand-assembled using individually cut foamcore panels taped together with painter's tape to ensure structural integrity and light sealing. Additional cutouts were made to allow cables from the integrating spheres and photodiodes to exit the enclosure and connect to lock-in amplifiers. A flap-style door was added to the rear of the box to permit manual access and visual inspection of the internal components, while a larger side opening allowed for the insertion and positioning of the syringe pump. These features ensured that the experimental system remained both functional and accessible while fully enclosed.
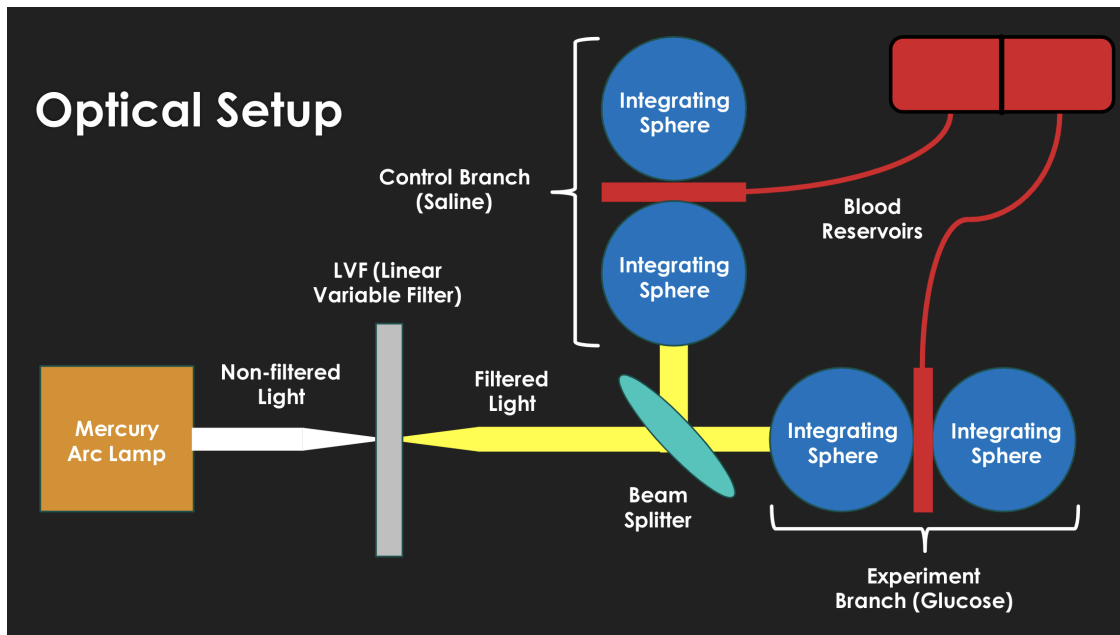
Figure 2.4 Schematic of the optical setup used in the bioptic experiment. The system includes a mercury arc lamp, linear variable filter (LVF), beam splitter, and two branches—one experimental (with glucose) and one control (with saline). Each branch contains two integrating spheres, with flow chambers located between them. The temperature control system was built to enclose and regulate the environment surrounding this setup. (Image courtesy of Jared Logan)

2.4   Insulation Improvements

Although the initial enclosure provided some thermal stability, it quickly became apparent that temperature control was compromised by heat leakage around the base and through cable ingress points. These gaps allowed warm air to escape and cooler ambient air to enter, making it difficult to maintain the elevated temperatures required for blood measurements.

Cotton balls were selected as the primary insulating material due to their low cost, flexibility, and strong thermal resistance. They were easy to cluster, reposition, and replace, and they conformed well to irregular seams and openings. For installation, cotton balls were hot glued together in dense clusters and then affixed to the bottom edges of the enclosure and around all cable entry points.

This approach created a passive but highly effective thermal seal, significantly reducing heat loss while maintaining accessibility to internal components. As a result, subsequent test runs showed improved heat retention and more consistent temperature readings across the thermistor network, as evidenced by the data presented in the Results chapter.

2.5 Heat Source and PID Control

Heating for the system was provided by a repurposed food dehydrator, selected for its compact form factor and ability to deliver steady, low-to-moderate heat. The heating element and fan assembly were integrated into the top of the enclosure, where warm air could be blown directly into the chamber and distributed throughout the internal volume.

An Arduino-based PID controller regulated the heating element, interfacing with a basic LCD screen and manual input controls to set and maintain a target temperature. The controller operated independently from the Python-based monitoring and logging software, which passively recorded temperature data from the thermistor network. This separation ensured that the heating system remained robust and stable even during extended runs.

The system was tuned through an iterative process in which the heat input value on the PID controller was gradually adjusted, each time observing the resulting internal temperature trends over extended durations. By varying the setpoint and monitoring the enclosure's thermal response, an optimal balance between input heat and retention was established. For the current configuration, setting the PID input to 50°C resulted in stable temperatures within the enclosure ranging from 36°C to 39°C across the experimental plane (see Figure 3.5). This tuning confirmed the system's ability to maintain physiologically relevant conditions over multiple hours, validating its suitability for future blood optical experiments.

2.6   Data Logging and Real-Time Monitoring

Temperature data from the six thermistors was continuously collected using a custom Python script (see Appendix A). This program iteratively cycled through each thermistor, capturing a new data point for each sensor every second. All temperature values were plotted in real time using matplotlib, providing a live graph for ongoing monitoring throughout experimental runs. Simultaneously, all data were logged to a CSV file that could be saved and exported at any time by interrupting the program.

Although the software did not include automated error handling, validation of the readings was straightforward. At room temperature, all thermistors typically registered in the low twenties Celsius, and once heating was initiated, the expected rise toward the 36°C to 40°C range provided a reliable confirmation that the system was functioning properly. Negative readings or implausible jumps were easily identifiable and could be discarded. Because heat input was managed separately by the Arduino PID controller, the Python software functioned purely as a passive monitoring and logging system. This separation of control and data acquisition added robustness to the design and reduced the likelihood of sensor noise.

Chapter 3

Results

The development of the temperature control system involved several rounds of refinement and testing, each aimed at resolving a specific technical challenge in the pursuit of stable thermal conditions. The effectiveness of these improvements can be demonstrated by examining temperature behavior across multiple test cases integrating the thermistor network and the fully assembled enclosure.

One of the earliest challenges encountered was signal interference among thermistor channels during simultaneous data acquisition. When the DAQ system attempted to collect values from all thermistors simultaneously, the data exhibited a phenomenon we liked to call "thermistor tugging," where a temperature spike in one channel appeared to influence the output of other thermistors that were not experiencing any real temperature change. This effect is shown in Figure 3.1, where individual sensors were sequentially heated by hand, and yet all five plotted thermistors exhibit subtle deflections around the same time, despite only one being actively altered.

To correct for this interference, the data acquisition protocol was revised such that thermistors were sampled one at a time in a repeating cycle (one thermistor read every second, thus a six-second cycle), rather than all at once. This change was implemented through a modification of the Python control script, allowing the system to wait between each reading and isolate individual sensor inputs. The success of this adjustment is shown in Figure 3.2, where similar sequential heating of

thermistors results in clean, isolated temperature changes with no measurable distortion in adjacent channels. This confirmed that the tugging was due to software timing and channel overlap, not hardware defects, and validated the integrity of the temperature data collected from that point forward.

With reliable temperature data now in place, attention shifted to the question of whether the system could sustain spatially consistent temperatures within the target range of 36°C to 40°C. The difference between the enclosure configurations with and without added cotton insulation was especially pronounced. Figure 3.4 shows the result of a 30-minute run using the enclosure without insulation. Although the system reached elevated temperatures, the spread among thermistor readings exceeded 10°C across the enclosure, indicating a significant gradient. This variation was present across the entire enclosure and not limited to any single structural element, implying that heat was escaping through multiple weak points and that warm air was not effectively circulating throughout the interior. The system lacked the thermal consistency required to simulate controlled physiological conditions.

After insulation was added—consisting of cotton balls lining the base and sealing each cable ingress point—the system demonstrated a dramatic improvement in thermal uniformity. The final insulated configuration is shown in Figure 3.5, where all thermistors located in the experimental plane (excluding T2, which was in contact with the optical table) maintained a narrow temperature band between 36°C and 39°C (see Figure 3.3 for spatial placement).This spread of only 2°C contrasts sharply with the uninsulated case and reflects a substantial gain in spatial consistency. T1 and T3 through T6, all placed directly in the region where blood flows during experiments, exhibited the most stable temperature readings.

These results confirm that the final system met its performance targets: stable temperature within the desired range, spatial uniformity across the experimental plane, and clean, interference-free data acquisition.
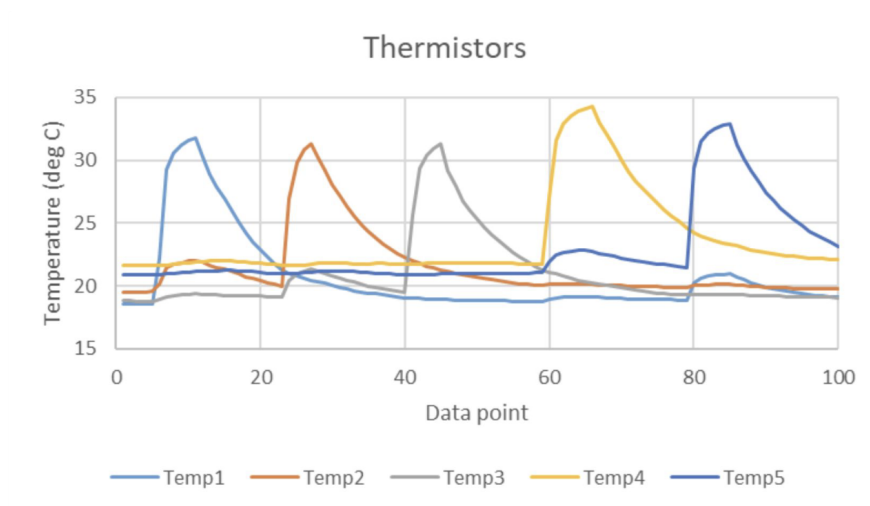
Figure 3.1 Thermistor data showing signal interference during simultaneous sampling. For example, when T1 experiences a sudden temperature spike—such as from being touched by a human hand—T2 exhibits a small but synchronized rise, despite no actual change in its environment. Similar reactive artifacts can be observed across other channels as well. This behavior illustrates data crosstalk caused by the DAQ attempting to read from all thermistors simultaneously.
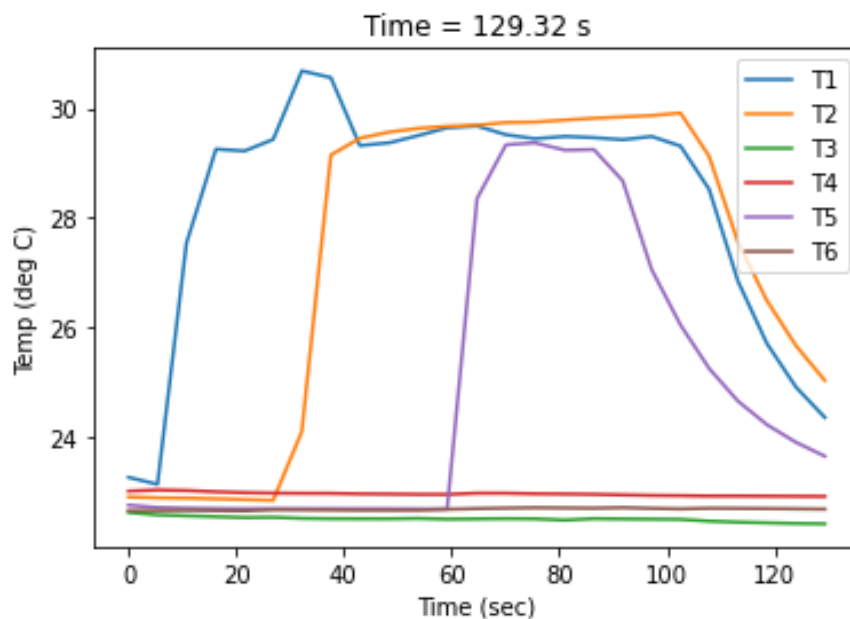

Figure 3.2 Thermistor response after code modification. Each sensor registers isolated heating events with no distortion in other channels, confirming the resolution of crosstalk.
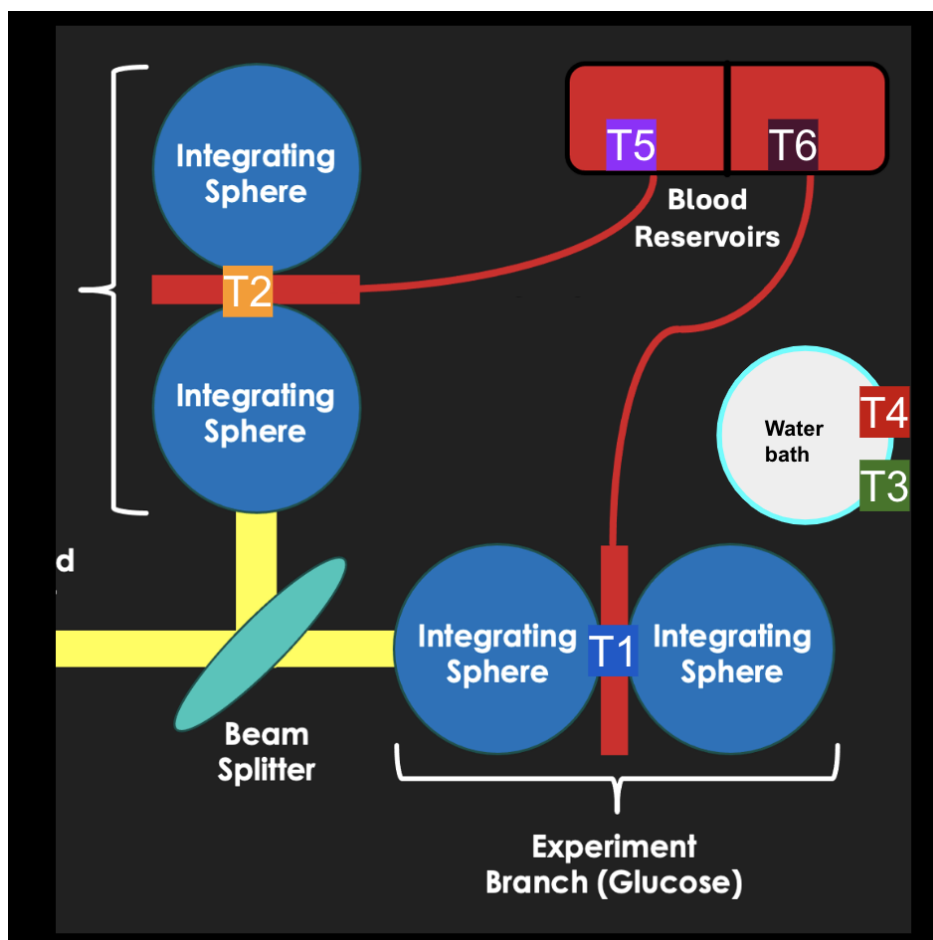
Figure 3.3 Diagram of thermistor placement within the experimental setup. The flow chambers are oriented vertically; T1 rests atop the flow chamber in the experimental branch (approximately four inches above the optical table), while T2 is positioned directly beneath the flow chamber of the control branch (in contact with the optical table). Despite T3 being above and vertically seperated from T1 by about 3 inches (resting on top of the water bath), they report similar temperatures under insulated conditions. T4, also atop the water bath, shares the same elevation as T3. T5 and T6 are located on the syringe pump housing near their respective syringes, roughly 1–1.5 inches below the height of T1.
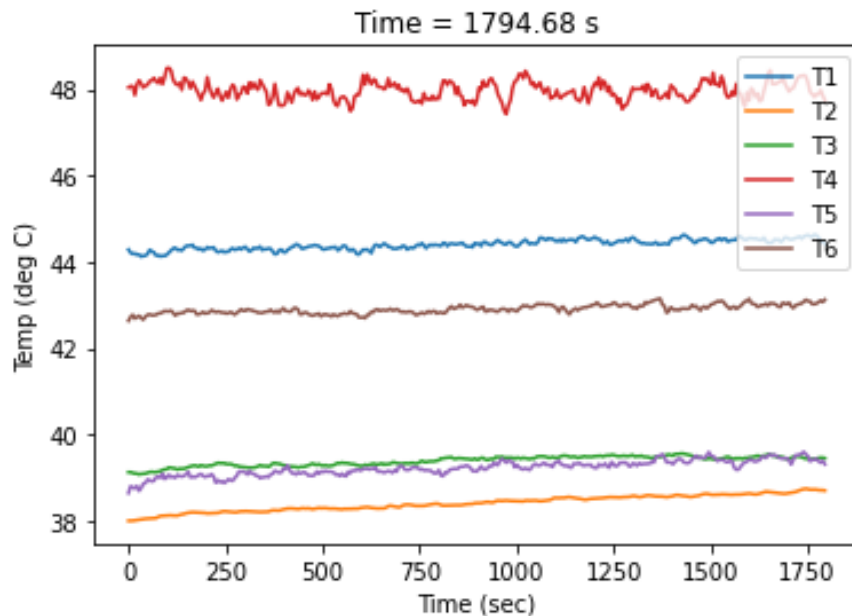
Figure 3.4 Long-duration temperature profile of the enclosure without cotton insulation. T1 and T3, located at the plane of blood flow, show vastly different temperatures (a separation of a little over 8 degrees). T2 remained lower due to contact with the metal optical table, and yet is closer to the temperature of T2 than would be desired in such an enclosure. Ideally, T1 and T3 should be much closer (laying in the same horizontal plane within the box).
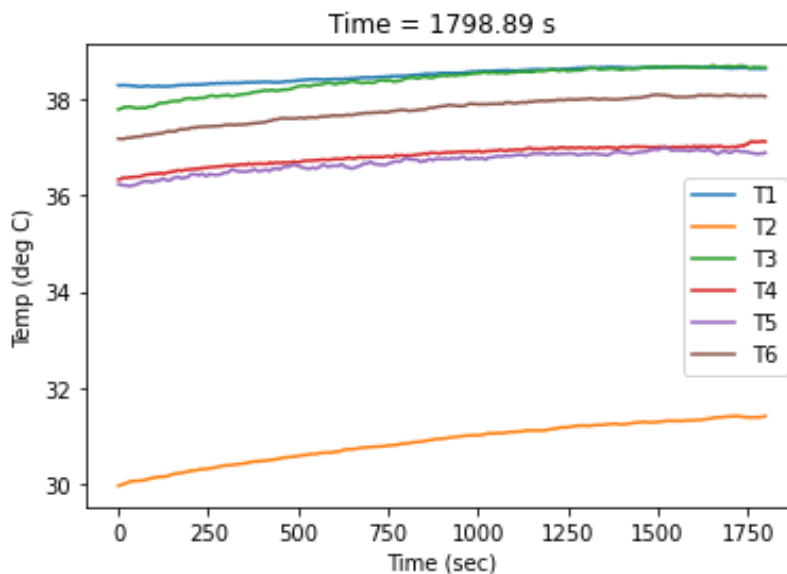
Figure 3.5 Long-duration temperature profile of the insulated enclosure. T1 and T3, located at the plane of blood flow, maintained stable temperatures near 38°C. T2 remained lower due to contact with the metal optical table. The temperature of the tubing immediately upstream and downstream of each flow chamber may also vary slightly due to differences in elevation, which can affect localized air temperature and heat exposure.

Chapter 4

Discussion

The results of this project demonstrate that the constructed temperature control system effectively addresses the core design goals of maintaining physiologically relevant temperatures, achieving spatial consistency across the experimental plane, and enabling stable performance over extended experimental durations. Through a combination of mechanical insulation, airflow management, and software refinements, the system achieved temperature control within the biologically relevant range of roughly 36°C to 38°C across multiple points in the experimental region. The validation of the thermistor array, resolution of DAQ interference, and successful retention of heat within the enclosure collectively indicate that the system is suitable for long-duration experiments involving live biological fluids, such as whole blood.

One of the most important improvements made during development was the elimination of thermistor interference. The decision to move from simultaneous data acquisition to a sequential sampling routine proved crucial, as it prevented channel overlap and data corruption that would have otherwise compromised experimental integrity. This adjustment also highlights the importance of software design in the context of physical measurement systems, especially when working with constrained hardware like basic thermistors and affordable DAQ systems. The stability demonstrated

in the corrected data logs suggests that even inexpensive temperature sensors can yield high-quality results if integrated and processed appropriately.

The comparison between test runs with and without added cotton insulation provides further insight into the physical dynamics of the enclosure. The uninsulated system suffered from wide thermal gradients—over 10°C in some cases—which would have introduced significant spatial variability in blood temperature and made consistent measurement difficult. In contrast, the insulated system maintained a narrow spread of approximately 2°C across all thermistors in the experimental plane. This improvement is particularly meaningful given the sensitivity of biological processes and optical properties to temperature fluctuations. The results also validate the decision to use cotton balls, proving that simple design interventions can yield substantial performance gains when strategically applied.

Despite these successes, several limitations remain. First, the current design relies on a manually tuned heat source controlled by an Arduino PID, which, while effective, does not communicate directly with the temperature logging software. This separation introduces a degree of lag and makes it difficult to implement automated feedback control. Future iterations of the system could consider a fully integrated temperature regulation loop, in which real-time thermistor data directly informs heating input (although this introduces more complexity to the system, which may increase likelihood of systemic bugs). This would allow for more precise control and eliminate the need for manual oversight during long experiments.

The design of the fan-driven heat distribution system also deserves further optimization. Although it proved effective in distributing heat evenly throughout the enclosure, it currently lacks quantitative airflow validation. Additional measurements of air velocity or temperature distribution in three dimensions could inform future improvements in circulation and pressure management, particularly if higher levels of spatial uniformity are required. Future fluid measurements may also warrant insulating the lower fluid tubing entering the flow chambers, where vertical positioning

and thermal conduction could lead to unintended heat loss before and after the blood reaches the experimental region.

Ultimately, this project demonstrates that a thermally stable and spatially uniform environment for bioptics experiments can be achieved using accessible tools and materials. The system provides a robust foundation for future studies that aim to investigate temperature-dependent optical properties of whole blood and other biological tissues, particularly in experimental conditions that require both precision and long-duration thermal regulation.

Appendix A

Thermistor Temperature Sampling Script

The Python script below was used to acquire voltage data from six thermistors using NI-DAQ hardware, compute their resistances, and convert the values to temperatures using the Steinhart-Hart equation. Real-time plotting was also included for live monitoring.

Listing A.1 Thermistor Sampling Script

```
import matplotlib.pyplot as plt

import numpy as np

import nidaqmx

import time

from nidaqmx.constants import TerminalConfiguration


\begin{lstlisting}[language=Python, basicstyle=\footnotesize\ttfamily, caption={Thermi

import matplotlib.pyplot as plt

import numpy as np

import nidaqmx

import time

from nidaqmx.constants import TerminalConfiguration


def make_file(timepoints, temperatures, fileName1):
```

```python
    titles = [["Time", "Temp1", "Temp2", "Temp3", "Temp4", "Temp5", "Temp6"]]
    out = titles + np.hstack((timepoints.reshape(-1, 1), temperatures)).tolist()
    np.savetxt(fileName1, out, fmt='%s', delimiter=',')


try:
    NC = 6
    rate = 1000
    spc = 1000
    time_limit = 1800
    temperatures = []
    timepoints = []


    R_values = [98250, 96900, 98200, 97720, 98060, 98200]


    steinhart_coeffs = [
        [0.000532378686, 0.000241446832, 2.73484069e-8],
        [0.000516641570, 0.000243501154, 2.21696409e-8],
        [0.00422409009, -0.000260185386, 1.38829929e-6],
        [0.00103865504, 0.000172494711, 2.13628021e-7],
        [0.00138823400, 0.000125998827, 3.36968690e-7],
        [0.00473919375, -0.000327699874, 1.55871365e-6]
    ]


    elapsed_time = 0
    start_time = time.time()


    with nidaqmx.Task() as ao_task:
        ao_task.ao_channels.add_ao_voltage_chan("Dev2/ao0", min_val=0, max_val=5)
        ao_task.write(5.0)
```

```
while elapsed_time < time_limit:

    elapsed_time = time.time() - start_time

    if elapsed_time >= time_limit:

        break


    timepoints.append(elapsed_time)

    temp_row = [None] * NC


    for j in range(NC):

        with nidaqmx.Task() as task:

            task.ai_channels.add_ai_voltage_chan(

                "Dev2/ai1", terminal_config=TerminalConfiguration.BAL_DIFF, min_va

            )

            task.ai_channels.add_ai_voltage_chan(

                f"Dev2/ai{j + 2}", terminal_config=TerminalConfiguration.BAL_DIFF,

            )


            task.start()

            yin = task.read(number_of_samples_per_channel=spc)

            task.stop()


            Vin = np.average(yin[0])

            Vout = np.average(yin[1])


            Rt = R_values[j] * (Vin / Vout - 1)

            if Rt <= 0:

                Rt = 0.01

                print(f"Resistance {j+1} tried to be negative!")


            a, b, c = steinhart_coeffs[j]
```

```python
            TempK = 1 / (a + b * np.log(Rt) + c * (np.log(Rt))**3)
            TempC = TempK - 273.15
            temp_row[j] = TempC

        temperatures.append(temp_row)


        plt.clf()
        for k in range(NC):
            temp_data = [t[k] for t in temperatures if t[k] is not None]
            plt.plot(timepoints[:len(temp_data)], temp_data, label=f'T{k+1}')
        plt.xlabel('Time␣(sec)')
        plt.ylabel('Temp␣(deg␣C)')
        plt.legend(loc='best')
        plt.title(f'Time␣=␣{elapsed_time:.2f}␣s')
        plt.draw()
        plt.pause(0.01)


        time.sleep(1)

except Exception as e:
    raise e
```

Bibliography

[1] Yaroslavsky, A. N., Schulze, P. C., Yaroslavsky, I. V., Schober, R., Ulrich, F., & Schwarzmaier, H. J. (1996). Optical properties of human cranial bone in the 650–950 nm spectral range. *Physics in Medicine and Biology*, 41(8).

[2] Amerov, A. K., Arnold, M. A., & Small, G. W. (1999). Near-infrared spectroscopic analysis of blood glucose in mixtures with multiple interferents. *Journal of Biomedical Optics*, 4(1).

[3] Bosschaart, N., Edelman, G. J., Aalders, M. C., & van Leeuwen, T. G. (2008). A literature review and novel theoretical approach on the optical properties of whole blood. *Physiological Measurement*, 29(6).

[4] Hale, G. M., & Querry, M. R. (1973). Optical constants of water in the 200-nm to 200-μm wavelength region. *Applied Optics*, 12(3).

[5] Friebel, M., & Meinke, M. (2005). Model function to calculate the refractive index of native hemoglobin in the visible and near-infrared spectral range. *Applied Optics*, 44(3).

[6] Sfareni, C., & Quaresima, V. (1997). Temperature dependence of near-infrared spectra of hemoglobin derivatives. *Journal of Biomedical Optics*, 2(4).

[7] Collins, E. J. (1925). Change in the Infra-Red Absorption Spectrum of Water with Temperature. *Physical Review*.

[8] Hammer, M., Schweitzer, D., Michel, B., Thamm, E., & Kolb, A. (1998). Single scattering by red blood cells. *Applied Optics*.

[9] Steinke, J. M., & Shepherd, A. P. (1992). Effects of temperature on optical absorbance spectra of oxy-, carboxy-, and deoxyhemoglobin. *Clinical Chemistry*.

[10] Bradley, A. F., & Stupfel, M. (1956). Effect of temperature on P_{CO_2} and P_{O_2} of blood in vitro. *Journal of Applied Physiology*.

[11] Harkness, J., Roth, J., Logan, J., Vanfleet, R., Davis, R., Pitt, W., & Westover, T. (2025). Optical changes in whole blood versus glucose concentration. In *Proceedings of Biomedical Light Scattering XV* (Vol. 13320, Paper 133200H). https://doi.org/10.1117/12.3043970

Index